Climate Dynamics
https://doi.org/10.1007/s00382-018-4530-7

Stable oxygen isotopes in Romanian oak tree rings record summer droughts and associated large-scale circulation patterns over Europe

Viorica Nagavciuc[1,2,3,4] · Monica Ionita[5] · Aurel Perşoiu[4,6] · Ionel Popa[7] · Neil J. Loader[8] · Danny McCarroll[8]

Received: 17 May 2018 / Accepted: 8 November 2018

Abstract
We present the first annual oxygen isotope record (1900–2016) from the latewood (LW) cellulose of oak trees (*Quercus robur*) from NW Romania. As expected, the results correlate negatively with summer relative humidity, sunshine duration and precipitation and positively with summer maximum temperature. Spatial correlation analysis reveals a clear signal reflecting drought conditions at a European scale. Interannual variability is influenced by large-scale atmospheric circulation and by surface temperatures in the North Atlantic Ocean and the Mediterranean Sea. There is considerable potential to produce long and well-replicated oak tree ring stable isotope chronologies in Romania which would allow reconstructions of both regional drought and large-scale circulation variability over southern and central Europe.

Keywords Oak · $\delta^{18}O$ · Relative humidity · Dendrochronology · Atmospheric circulation

1 Introduction

European droughts and heat waves have increased in frequency and intensity in the twenty-first century (van Lanen et al. 2016; Ionita 2015; Ionita et al. 2017), leading to increased risks to human health, property and infrastructure. Climate models suggest that rising global temperatures will lead to more frequent and stronger heat waves and summer droughts in the coming century, with southeastern Europe being particularly affected (Spinoni et al. 2015). The triggering mechanisms behind the genesis and dynamics of heat waves are complex (Kingston et al. 2015; Ionita et al. 2017), and existing observational data are insufficient to offer robust explanations. There is thus a need to look for alternative sources to reconstruct hydroclimatic variability on multi-centennial and longer timescales (Jones and Mann 2004; Huber and Gulledge 2011; Smerdon and Pollack 2016). Tree rings are well established archives of paleoclimatic information, with the advantages of length, annual resolution, precise dating and varied geographical distribution (Schweingruber 1996). However, robust reconstructions of past climate based on measures of tree growth, such as ring width, are restricted to areas where growth is strongly limited by a single well-definable climatic controller. Typically this is summer temperature at high altitudes/latitudes (Popa and Kern 2009; Popa and Bouriaud 2013; Nechita et al. 2017)

Electronic supplementary material The online version of this article (https://doi.org/10.1007/s00382-018-4530-7) contains supplementary material, which is available to authorized users.

✉ Viorica Nagavciuc
nagavciuc.viorica@gmail.com

1 Faculty of Forestry, Ştefan cel Mare University, Suceava, Romania

2 Institute for Geological and Geochemical Research, Research Centre for Astronomy and Earth Sciences, Hungarian Academy of Sciences, Budapest, Hungary

3 Departement of Geography, Johannes Gutenberg University, Mainz, Germany

4 Stable Isotope Laboratory, Ştefan cel Mare University, Suceava, Romania

5 Paleoclimate Dynamics Group, Alfred-Wegener-Institute for Polar and Marine Research, Bussestrasse 24, 27570 Bremerhaven, Germany

6 Emil Racoviță Institute of Speleology, Romanian Academy, Cluj-Napoca, Romania

7 National Research and Development Institute for Silviculture Marin Drăcea, Câmpulung Moldovenesc, Romania

8 Department of Geography, College of Science, Swansea University, Singleton Park, Swansea SA2 8PP, UK

Published online: 20 November 2018

and precipitation or related hydroclimatic variables in very dry environments (Popa and Sidor 2010; Kern et al. 2012; Levanič et al. 2013; Árvai et al. 2018). Measures of tree ring density (Grudd 2008; Kłusek et al. 2015), and the related property of blue reflectance (McCarroll et al. 2002; Wilson et al. 2014), can provide even stronger climatic signals, but are limited to conifers. In contrast, the $^{18}O/^{16}O$ ratio in tree rings is not dependent on net growth, but acts as a passive monitor of environmental change (McCarroll and Loader 2004; Leavitt 2010; Gagen et al. 2011; Young et al. 2015), potentially providing paleoclimate information for regions that are not close to an ecological limit (Haupt et al. 2011; Labuhn et al. 2016). The $\delta^{18}O$ values in tree ring cellulose depend on the stable isotope composition of the water taken up by roots, evaporative enrichment in the leaves and on biological fractionation and isotopic exchange occurring during photosynthesis and cellulose formation (McCarroll and Loader 2004; Gessler et al. 2013; Treydte et al. 2014). The $\delta^{18}O$ values in soil water are directly influenced by those in precipitation, in turn controlled by atmospheric circulation patterns, condensation temperature, precipitation amount and relative humidity (Dansgaard 1964). The dominant control on the enrichment of leaf water in the heavy isotopes is the difference in vapour pressure of leaf air and ambient air, which is controlled by relative humidity (Gessler et al. 2013; Labuhn et al. 2016). Dry and hot climate conditions lead to an enrichment in ^{18}O due to evaporation, yielding higher $\delta^{18}O$ values in tree-ring cellulose (Labuhn et al. 2016). The dominant environmental signals in tree ring oxygen stable isotope ratios are thus the stable isotope composition of precipitation and summer relative humidity (McCarroll and Loader 2004; Labuhn et al. 2014; Young et al. 2015).

In terms of dendrochronological series, Romania has a high potential to develop a well-replicated oak chronology covering almost the entire Holocene using the wood from the well-preserved oak forests together with abundant archaeological and sub-fossil oak timbers (Rădoane et al. 2015; Kern and Popa 2016; Nechita et al. 2017). This region is characterized by limited tree-ring-based climate reconstructions (Luterbacher et al. 2016), because tree ring widths are poorly correlated with climate (Nechita and Popa 2012; Nechita 2014). Strong paleoclimate reconstructions from this part of south-eastern Europe, where Atlantic, Mediterranean and Scandinavian climatic influences converge, would fill a clear gap in the paleoclimatic data network of Europe.

This study aims to evaluate the potential of oxygen isotopes in oak tree rings from Romania for producing long records of hydroclimate, including summer drought, and to assess whether the local variations in stable oxygen isotope ratios are linked to large-scale atmospheric circulation patterns over Europe.

2 Data and methods

2.1 Study area and meteorological data

The Nușfalău sampling site is situated in north-western Romania, 47.19°N, 22.66°E, 270 m above sea level, (Fig. 1). The local climate is temperate-continental, with mild winters, hot, dry summers and westerlies dominating the atmospheric circulation. Local meteorological data for the period 1961–2013 CE are available from the Romanian Meteorological Administration station Oradea (47.04°N, 21.91°E), 60 km west of the study site. The meteorological data includes: maximum (T_{max}), mean (T_{mean}), minimum (T_{min}) and soil temperature (T_{soil}), sunshine duration (SS), cloud cover (CC), relative humidity (RH), and precipitation amount (PP). Highest monthly precipitation amounts occur in June (78.26 mm on average), and the highest maximum temperatures are recorded in July (27.23 °C on average) and August (27.26 °C on average). Over the 1961–2013 period, the highest precipitation amount was recorded in June 1980 (178.56 mm), and the highest monthly maximum temperature was recorded in July 2012 (32.07 °C). The lowest relative humidity occurs throughout the summer months (June—71.63% and July—69.60%).

2.2 Gridded climate data

Gridded precipitation amount totals, T_{mean} and the self-calibrated Palmer Drought Severity Index (scPDSI) covering 1901–2014 CE were extracted from the monthly CRU T.S. 4.01 dataset (Harris et al. 2013), with a spatial resolution of 0.5°×0.5°. To investigate links with Northern Hemisphere atmospheric circulation we used the seasonal means of geopotential height at 500 mb (Z500), zonal wind (U500) and meridional wind (V500) at 500 mb from the Twentieth century reanalysis (V2) data set (NCEPv2; Whitaker et al. 2004; Compo et al. 2006, 2011) on a 2°×2° grid, for the period 1901–2014 CE. The vertically integrated water vapor transport (WVT) (Peixoto and Oort 1992) was calculated through zonal wind (u), meridional wind (v) and specific humidity (q), from the same data set. WVT vectors for latitude (ϕ) and longitude (λ) are defined as follows:

$$\vec{Q}(\lambda, \phi, t) = Q_\lambda \vec{i} + Q_\phi \vec{j}, \tag{1}$$

where zonal (Q_λ) and meridional (Q_Φ) components of Q are given by Eq. (2):

$$\begin{aligned} Q_\lambda &= \int_0^{p_0} qu \frac{dp}{g} \\ Q_\phi &= \int_0^{p_0} qv \frac{dp}{g}, \end{aligned} \tag{2}$$

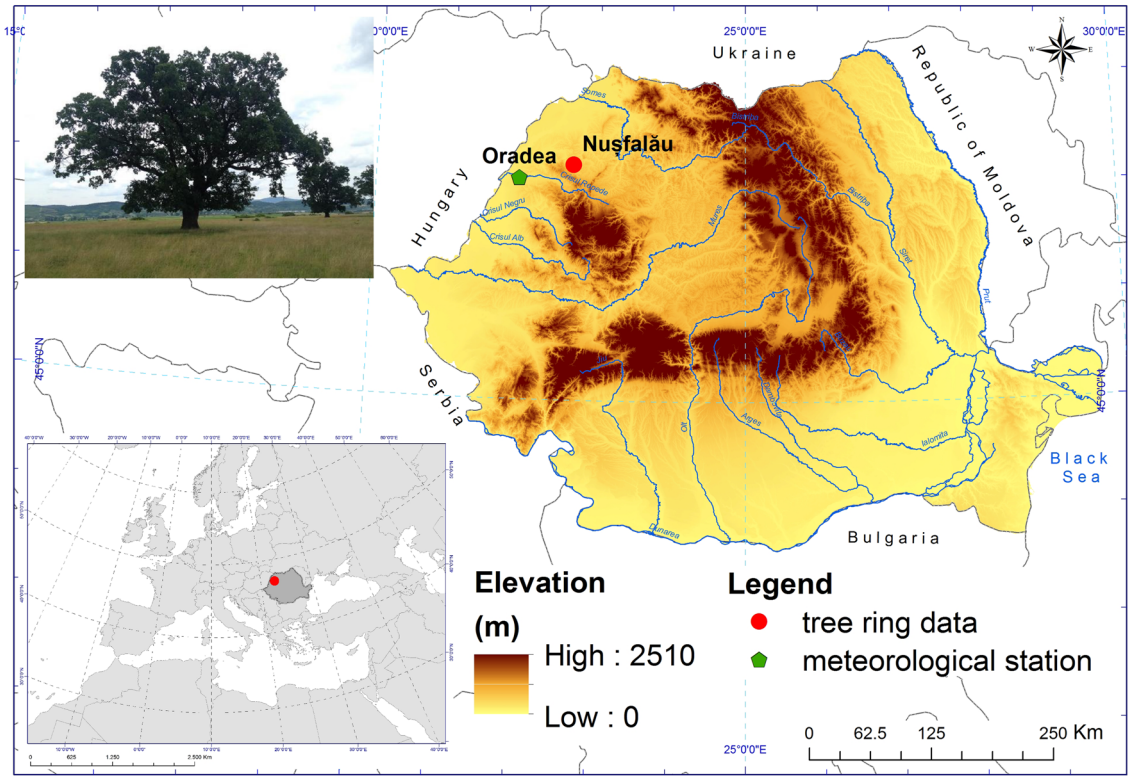

Fig. 1 Location of the sampling site and the nearby meteorological station (Oradea), and an image of a typical oak tree in this area

where q = specific humidity, u = zonal wind, v = meridional wind and p = pressure. The WVT is obtained by summation of water transport for all layers located between the Earth's surface and 300 hPa, above which the specific humidity in the twentieth century reanalysis (V2) model is zero (Kalnay et al. 1996; Whitaker et al. 2004; Compo et al. 2006, 2011). For sea surface temperature we used the 1° × 1° Hadley Centre Sea Ice and Sea Surface Temperature data set—HadISST (Rayner 2003).

2.3 Development of tree-ring chronologies and statistical methods

Two 5 mm increment cores were collected from each of ten oak trees (*Quercus robur* L.) in August 2016 at Nușfalău using standard dendrochronological sampling methods (Schweingruber 1988). One core per tree was fixed in a wooden support, polished, scanned and ring widths measured using the CDendro software, with a precision of 0.01 mm. Cross dating was performed and verified using COFECHA software (Holmes 1983). For stable isotope analysis, nine of the unmounted cores were manually dissected with a scalpel under magnification and the latewood (summer-wood) sections pooled into one sample. The earlywood is excluded, because in *Q. robur*, earlywood vessels are formed about 2–3 weeks before bud burst and are completed before full leaf expansion (Puchałka et al. 2017). Alpha-cellulose was extracted from latewood samples following the method of Boettger et al. (2007) and Loader et al. (1997) and homogenized using a Hielscher ultrasonic device (Laumer et al. 2009). For each sample, 0.30–0.35 mg of cellulose were packed in silver capsules, freeze-dried and pyrolyzed using a Thermo Scientific Flash High-Temperature Elemental Analyzer (HTEA) and isotope ratios were measured on the evolved CO_2 using a Delta V Advantage IRMS in the Stable Isotope Laboratory at Swansea University. Every tenth sample was measured three times, the analytical error being less than 0.3‰. The results are expressed using the conventional δ (delta) notation in per mil (‰) relative to the Vienna Standard Mean Ocean Water (VSMOW) standard (Coplen 1994).

Linear correlations between $\delta^{18}O$ and local monthly and seasonal climate parameters were explored using the Treeclim R package (Dalgaard and R Development Core Team 2010), with confidence intervals calculated using the bootstrap method. To identify connections with large-scale atmospheric circulation and North Atlantic Ocean sea surface temperature (SST), we constructed composite maps of Z500 and SST standardized anomalies for the summer season by selecting the years when the value of normalized time

series of $\delta^{18}O$ values was > 1 standard deviation (high) and < − 1 standard deviation (low), respectively. These thresholds were chosen as a compromise between the strength of the climate anomalies linked to $\delta^{18}O$ anomalies and the number of maps that satisfy this criterion. Further analysis has shown that the results are not sensitive to the exact threshold value used for the composite analysis (not shown). The significance of the composite maps is based on a standard *t* test (confidence level 95%).

3 Results and discussions

3.1 Local climate signal and links to regional patterns

As expected in samples from a temperate-continental region, the $\delta^{18}O$ values are significantly (95% significance level) and positively correlated with local summer (June–July–August, JJA) sunshine duration (r = 0.55) and maximum temperatures (r = 0.48) and significantly negatively correlated with summer cloud cover (r = − 0.49) and precipitation amount (r = − 0.51). The strongest correlation, however, is with the most direct control on oxygen isotope fractionation in the leaf, which is summer relative humidity (r = − 0.67). The calibration model passes standard split-period verification statistics (NCR 2006), including reduction of error (RE) and coefficient of efficiency (CE) (Table 1), suggesting that the relationship is temporally stable, and the correlation is strong enough to justify a variance-scaled reconstruction, so that past extremes are not routinely underestimated (McCarroll 2015). Given the short meteorological data set, the calibration—validation approach is supported by the results of a bootstrap approach to verification with 95% confidence limits (Fig. 2).

The spatial validity of the relationship between $\delta^{18}O$ ratio and summer precipitation, drought conditions and temperature was also analyzed, over the period 1901–2016. The $\delta^{18}O$ values record both local signals (Figure S1, Table 2) and signals at a European scale.

Table 1 Calibration and verification statistics between $\delta^{18}O$ and relative humidity in JJA

Calibration	Verification	r	R^2	RE	CE
1961–1986		0.49	0.24		
	1986–2013	0.73	0.53	0.50	0.45
1987–2013		0.73	0.53		
	1961–1985	0.51	0.26	0.32	0.16
Full period		0.67	0.45		

r correlation coefficient, R^2 coefficient of determination, *RE* reduction of error, *CE* coefficient of efficiency

Significant correlations with summer PP (Fig. 3a) extend over a wide area, with negative correlations over the whole of southern and central Europe and positive correlations over Fennoscandia. A similar dipole-like structure in the correlation analysis is found for the summer scPDSI index. High $\delta^{18}O$ values are associated with drought conditions over the central and the eastern part of Europe and wet conditions over Fennoscandia. The highest correlations are found over the eastern part of Europe (Fig. 3b). Strong spatial field correlations are found also for summer maximum temperature (Fig. 3c). High values of $\delta^{18}O$ are associated with hot summers over the whole of central and eastern Europe and cold summers over the northern part of Europe. The dipole-like structure identified in the correlation maps for PP and scPDSI is a well-known feature of summer hydroclimate at a European scale (Ionita et al. 2012; Ionita 2015). In general droughts and heat waves over the central and southern part of Europe are accompanied by prolonged wet and cold periods over the northern part of Europe, as in the summers of 1904, 1921, 1976 and 2015 (Ionita et al. 2012; Ionita 2015). This can be regarded as an indication that the $\delta^{18}O$ in tree rings for our site location is able to record not just dry/wet periods at a local scale, but is able to record also dry/wet periods at a European scale.

The highest correlation coefficients were found between $\delta^{18}O$ values and summer scPDSI field. As already indicated by the correlation analysis with local climate data (Table 2), $\delta^{18}O$ values are very sensitive to relative humidity and drought conditions. In order to better analyze the relationship between $\delta^{18}O$ and summer drought, a longer scPDSI series was extracted by averaging the gridded data over the region (20°E–25°E, 45°N–50°N). The temporal evolution of the $\delta^{18}O$ values and the scPDSI index is shown in Fig. 4a. The correlation coefficient between the two-time series is r = − 0.52 (p < 0.001) and prolonged dry periods (e.g. 1941–1950) are always associated with high values of $\delta^{18}O$. A striking feature of the $\delta^{18}O$ record is that it captures all of the extremely dry years (1954, 1976, 2003 and 2015), which were characterized by prolonged and extended droughts at a European scale (Ionita 2015; Spinoni et al. 2015; Ionita et al. 2017). The good agreement between the $\delta^{18}O$ record and the scPDSI time series and the results of the calibration model (Table 2) thus indicate that $\delta^{18}O$ values can be used as a proxy for the occurrence of dry/wet condition, especially over the eastern part of Europe.

To further explore the scPDSI signal in the $\delta^{18}O$ chronology, we compare the probability distribution function of $\delta^{18}O$ values for dry (scPDSI < − 2) and wet (scPDSI Index > 2) summers (Fig. 4b). The ± 2 threshold was chosen to focus just on the years that are characterized by extreme droughts. Values between − 2 and 2 for the scPDSI index indicate normal conditions, thus they are excluded from our

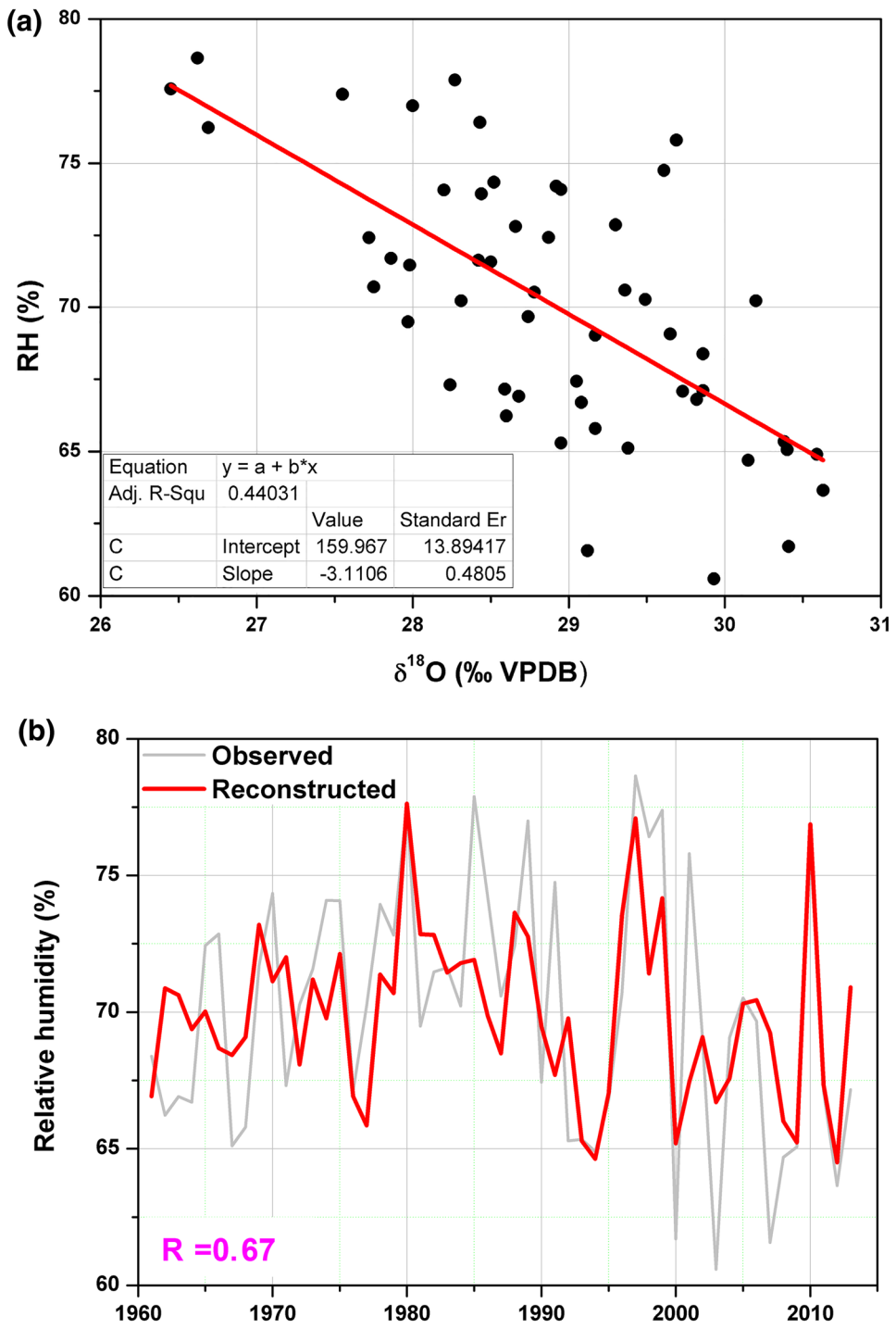

Fig. 2 **a** Regression of summer (JJA) relative humidity on $\delta^{18}O$ in the cellulose of late wood (LW) of oak tree-rings and **b** comparison between the observed (gray line) and the reconstruction (red line) mean summer relative humidity over the 1961–2013 period

analysis. The mean $\delta^{18}O$ value for the dry years (29.51‰) is significantly higher ($p < 0.001$) than the mean $\delta^{18}O$ value corresponding to wet years (28.13‰).

3.2 Moisture signal in the $\delta^{18}O$ values

Figure 5 shows the $\delta^{18}O$ time series, the seasonal cycle for precipitation and the daily maximum temperature for the instrumental period 1961–2013. Years recording the highest $\delta^{18}O$ values (> 1 standard deviation) and the lowest $\delta^{18}O$ years ($\delta^{18}O < -1$ standard deviation) (Fig. 5a) were selected and used to calculate the seasonal cycle in precipitation (Fig. 5b) and the daily maximum temperature (Fig. 5c). The blue lines (Fig. 5b) indicate the seasonal cycle for the years with high precipitation detected by low $\delta^{18}O$ values, while red lines show the seasonal cycle

Table 2 Calibration and verification statistics between $\delta^{18}O$ and scPDSI index in JJA

Calibration	Verification	r	R^2	RE	CE
1901–1958		0.53			
	1959–2016	0.52	0.27	0.28	0.26
1959–2016		0.52			
	1901–1958	0.53	0.28	0.27	0.26
Full period		0.52	0.28		

r correlation coefficient, R^2 coefficient of determination, *RE* reduction of error, *CE* coefficient of efficiency

for years with low precipitation as detected by high $\delta^{18}O$ values (Table S1). The black lines indicate the seasonal cycle computed over the period 1971–2000. As it can be inferred from Fig. 5b, wetter conditions than average (blue lines) are detected from May until August for the extreme low $\delta^{18}O$ values. In contrast, drier conditions (red lines) are detected from May to October in relationship with extreme high $\delta^{18}O$ values. For the daily maximum temperature (Fig. 5c) blue lines indicate that these years exhibit low daily maximum temperatures from June to August as detected by low $\delta^{18}O$ values. Red lines indicate that warm conditions prevail from May to August for years with high $\delta^{18}O$ values. The seasonal cycle analysis, for the extreme $\delta^{18}O$ values, indicates that there is no shift in the seasonal cycle for the extreme values, but there is a change in the absolute values of the analyzed variables. For example, the precipitation amount for low $\delta^{18}O$ values in May, June, July and August is more than double that recorded during the years with high $\delta^{18}O$ values. This verifies that the $\delta^{18}O$ in tree rings is able to capture the occurrence of extreme summers in terms of precipitation amount and temperature.

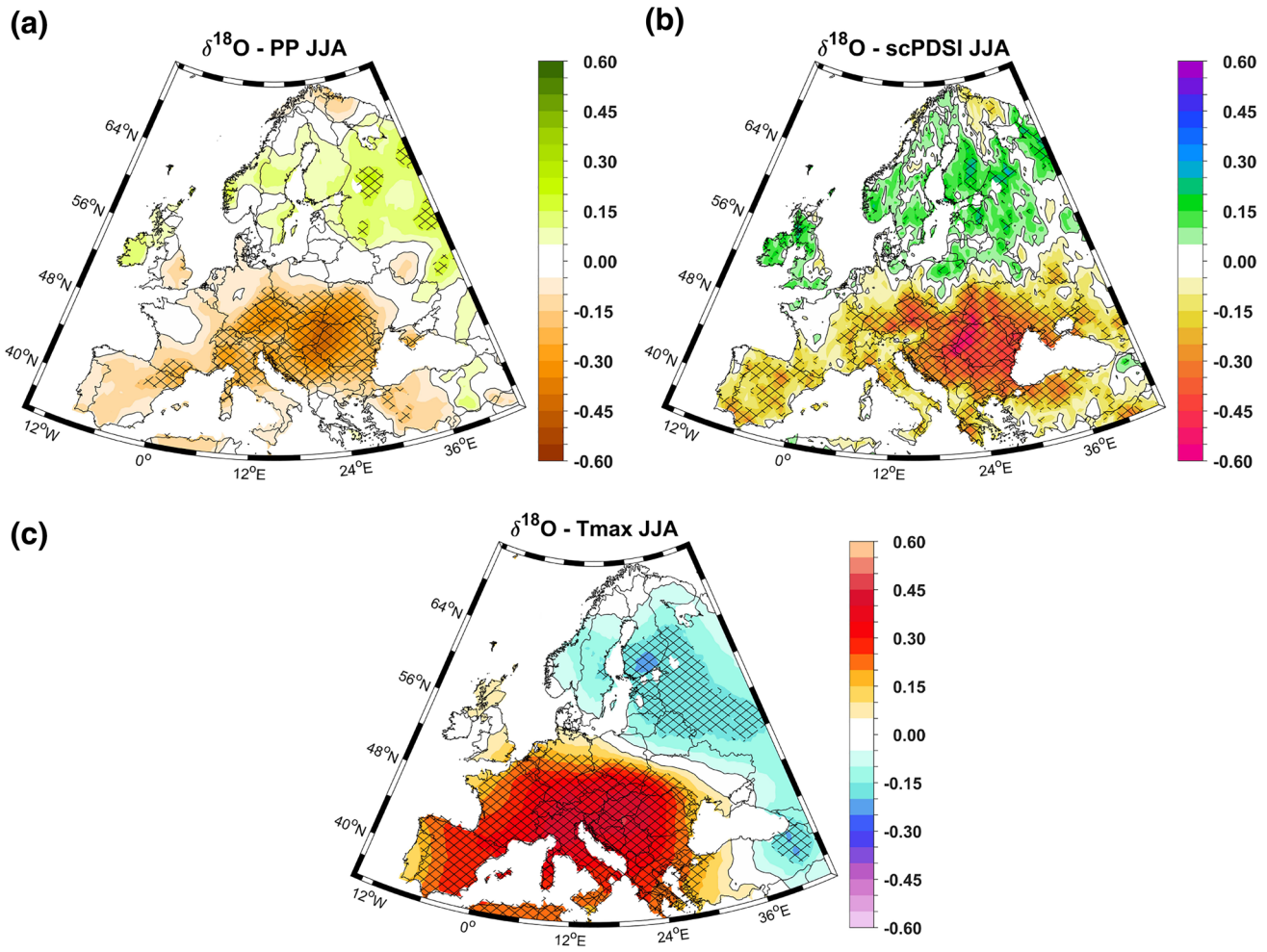

Fig. 3 **a** The spatial correlation map between $\delta^{18}O$ and: **a** summer precipitation; **b** summer scPDSI and **c** summer T_{max}. The hatching highlights significant correlation coefficients at a confidence level of 95%. Analyzed period: 1901–2014

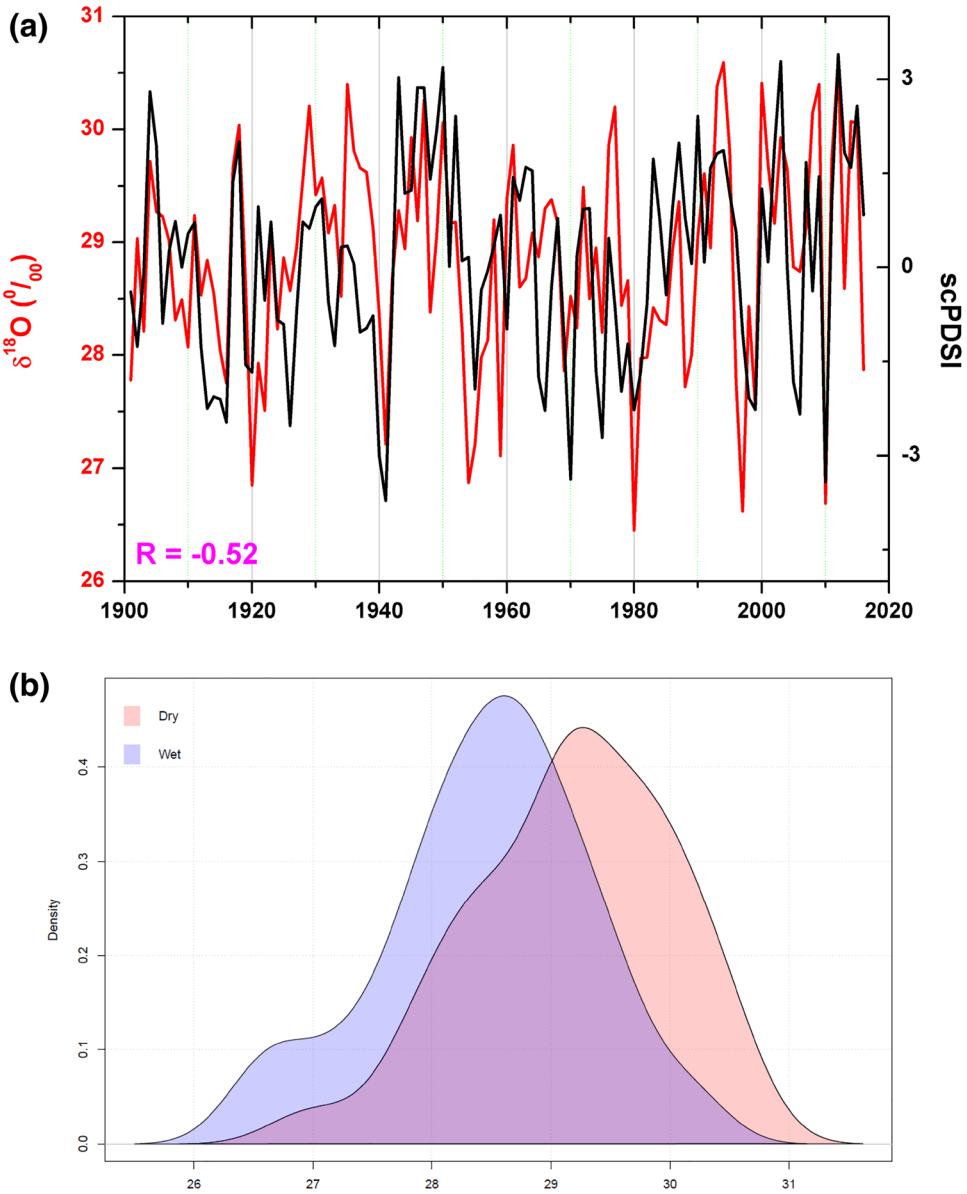

Fig. 4 **a** The temporal evolution of the $\delta^{18}O$ (red line) and the scPDSI index (black line) and **b** changes in the $\delta^{18}O$ probability density function for dry years (scPDSI index < -2) and wet years (scPDSI index > 2). In **a** the scPDSI index was multiplied by (-1) for a better comparison with the $\delta^{18}O$ time series

3.3 Tree ring oxygen isotope ratios and large-scale atmospheric circulation

The variations in the $\delta^{18}O$ values of tree rings have two major drivers: the stable isotope composition of the water absorbed through the roots and the evaporative enrichment of this water at the leaf surface (Roden et al. 2000). As the absorbed water is derived ultimately from precipitation, and its stable isotope composition can be controlled, inter alia, by atmospheric circulation (e.g. Gat 1996) we hypothesize that $\delta^{18}O$ of tree rings will be able to record the prevailing large-scale atmospheric circulation. In general, persistent dry (wet) conditions are associated with anticyclonic (cyclonic) circulation in summer, while the sea surface temperature at the moisture source delivered to NW Romania plays also an important role via the interaction with large-scale climatic or oceanic variability (Ionita et al. 2012; Schubert et al. 2014; Ionita 2015). To examine the relationship between $\delta^{18}O$ and large-scale atmospheric circulation we constructed composite maps using summer northern hemisphere geopotential height at 500 mb (Z500) and the vertically integrated water vapor transport (WVT). We focus on those years when the standardized (z-scored) $\delta^{18}O > 1$ standard deviation (High) and $\delta^{18}O < -1$ standard deviation (Low). The years that were used for the composite maps are shown in Table S1.

Low $\delta^{18}O$ values are associated with a Rossby wave train in the Z500 field, characterized by a low-pressure system over Greenland, followed by a high-pressure system in the central-north Atlantic Ocean, a low-pressure system located over the central part of Europe and a high-pressure

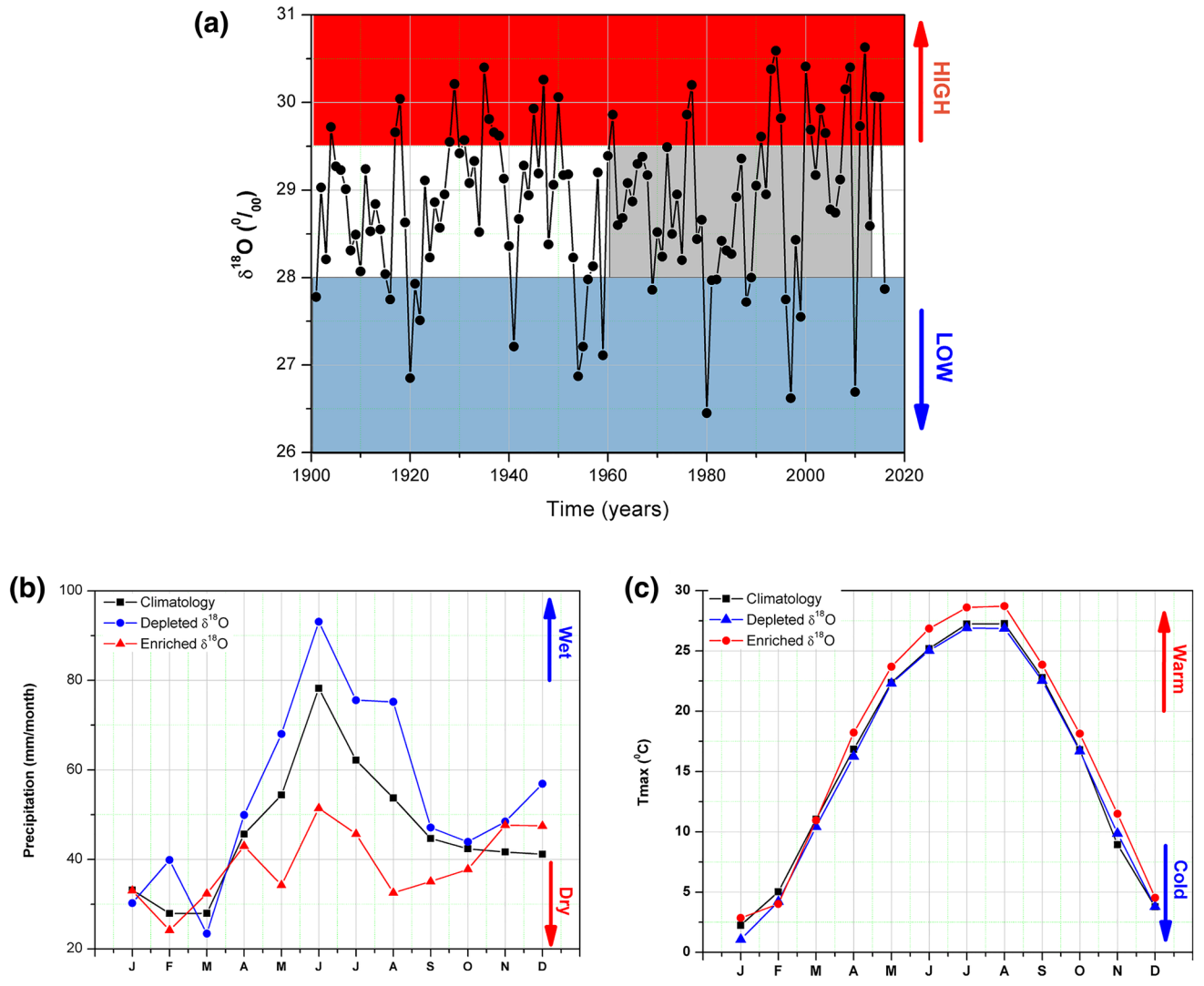

Fig. 5 **a** The temporal evolution of the $\delta^{18}O$ over the period 1900–2016; **b** the seasonal cycle for precipitation and **c** the seasonal cycle for the maximum temperature. **b, c** Average seasonal cycle (black line) and the seasonal cycles during years with extreme $\delta^{18}O$ values (red and blue shaded years in **a**). Analyzed period: 1961–2013

system over Fennoscandia and western Russia (Fig. 6a). This Rossby wave structure in the Z500 field enhances the advection of moisture from the Atlantic towards the central and eastern part of Europe (Fig. 6b). The enhanced moisture transport towards Europe is driven by the low-pressure system centered over Europe. Enhanced moisture advection leads to higher amounts of precipitation over the central and eastern part of Europe, which in turn will lead to low $\delta^{18}O$ values (amount effect, Dansgaard 1964). A similar pattern, in the Z500 field, is obtained when we compute the composite maps associated with wet summers, based on the scPDSI index (Figure S2a). Positive $\delta^{18}O$ values are recorded in association with a horse shoe-like block pattern with a low-pressure system over the central North Atlantic Ocean, a high-pressure system over the central part of Europe and a low-pressure system over western Russia (Fig. 6c). The anomalous Z500 center over Europe suggest a dominant subsidence and adiabatic warming associated with reduced cloudiness, heatwaves and reduced precipitation. The horse shoe-like block deflects the Atlantic storm tracks towards Fennoscandia (Fig. 6d). Warm summers and reduced precipitation will lead to $\delta^{18}O$ values (in agreement with the findings from Fig. 5), resulting from both the temperature effect of the stable isotope composition of precipitation and the potential sub-cloud evaporation of falling raindrops in a dry atmosphere. Strong evaporative enrichment at the leaf surface (as expected during warm and dry spells) would further enrich the water in ^{18}O over ^{16}O and drive $\delta^{18}O$ to higher values. Dry summers, as defined by the scPDSI index, are also associated with a similar horse shoe-like blocking

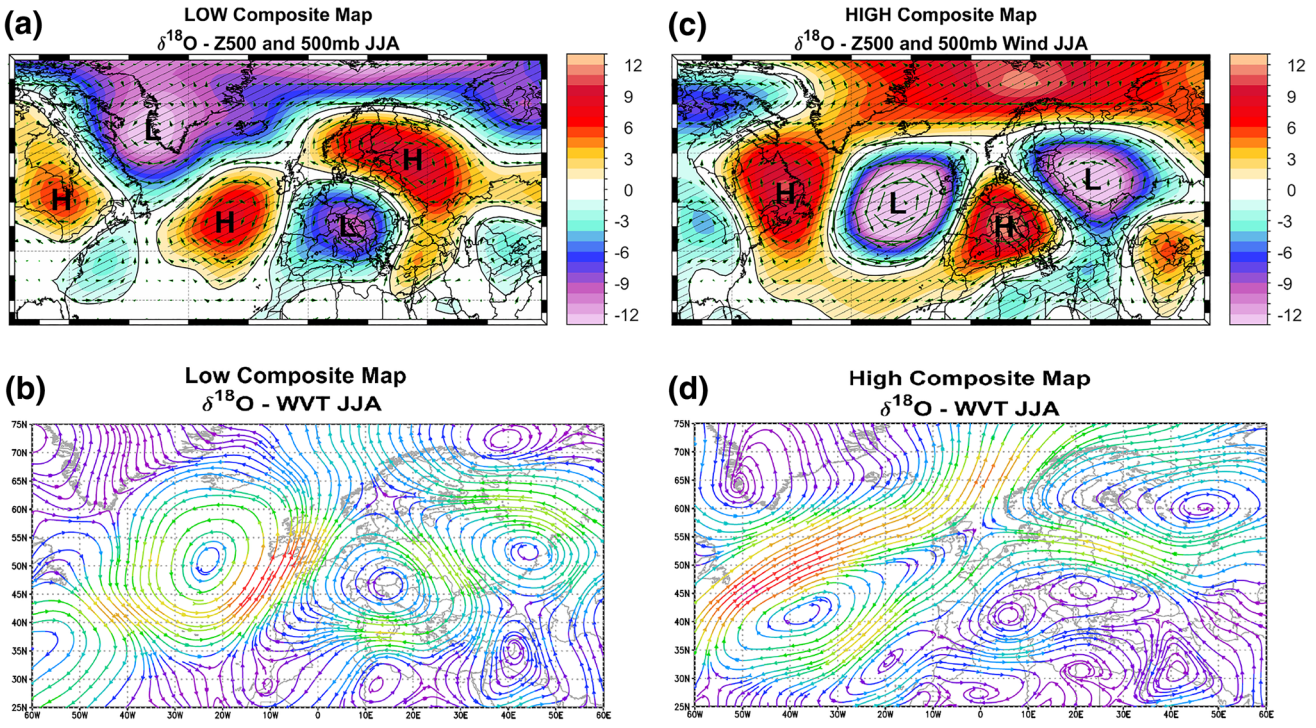

Fig. 6 **a** The composite map between low $\delta^{18}O$ (< −1 std. dev.) and summer Geopotential Height at 500mb (Z500—shaded areas) and summer 500 mb wind vectors (arrows); **b** the composite map between low $\delta^{18}O$ (< −1 std. dev.) and summer WVT; **c** the composite map between High $\delta^{18}O$ (>1 std. dev.) and summer geopotential height at 500 mb (Z500—shaded areas) and summer 500 mb wind vectors (arrows) and **d** the composite map between High $\delta^{18}O$ (>1 std. dev.) and summer WVT. The years used for the composite maps are shown in Table S1. Analyzed period: 1901–2014

pattern in the Z500 field (Figure S2b). From a long-term perspective, the Rossby wave-like structure identified in Fig. 6c was found to be associated with the occurrence of heat waves and extremely high summer temperatures over the central and eastern part of Europe (Ionita et al. 2017). This suggests that the inter-annual variability of our Romanian $\delta^{18}O$ record captures very well the spatial structure of a relatively typical large-scale climatological feature that produces droughts in the central and eastern part of Europe.

3.4 Tree ring oxygen isotope ratios and North Atlantic Ocean SST

Previous studies have emphasized the role of the Atlantic Ocean and the Mediterranean Sea SSTs in driving the occurrence of heat waves and droughts over the European region (Feudale and Shukla 2011; Ionita et al. 2012, 2017; Kingston et al. 2013; Ionita 2015). Following this line, significant correlations between $\delta^{18}O$ values and North Atlantic Ocean SST (Fig. 7a) indicate possible connections between the moisture availability over the eastern part of Europe and conditions at remote ocean areas. Positive $\delta^{18}O$ values are associated with positive SST anomalies in the North Atlantic Ocean, in a band stretching from 20°N to 40°N, the Mediterranean region and the Black Sea and negative SST anomalies in the central Atlantic Ocean. A similar SST pattern is found if we compute the correlation maps between the scPDSI index and the North Atlantic SST (Fig. 7b). Overall, the structure of the SST anomalies in Fig. 7 resembles the SST anomalies responsible for the occurrence of extreme drought events over the southern and eastern part of Europe (e.g. in 2003, 2015) (Van Lanen et al. 2016; Ionita et al. 2017). Ionita et al. (2017) have recently shown that warm Mediterranean SSTs have preceded and occurred concurrently with dry summers over most of the central and eastern part of Europe. In some particular years (e.g. summers of 2003 and 2015), extremely dry and hot summers over the central and eastern part of Europe, have occurred simultaneously with cold SST anomalies in the central Atlantic Ocean. In general, the North Atlantic Ocean SSTs anomalies can explain many features of the European droughts and heatwaves (Feudale and Shukla 2011). Mediterranean SSTs usually have an additional effect, with warm SST's acting to reduce the baroclinicity over the European region and reinforcing the blocking circulation. Altogether, when favorable phase conditions are met, both the large-scale atmospheric circulation and the SST act as a driver and/or precursor for the dry/wet conditions at a European scale. Overall, SST can modulate the tree ring cellulose

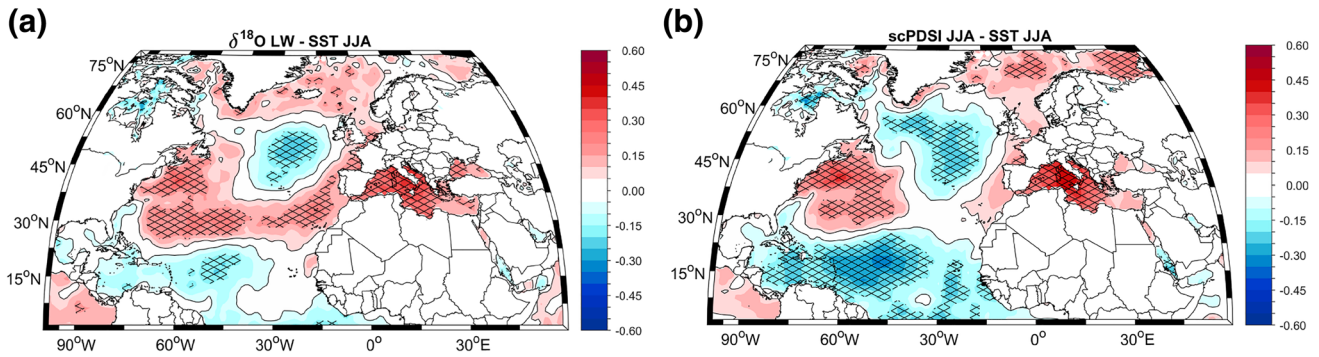

Fig. 7 **a** The correlation map between δ^{18}O LW and JJA SST and **b** as in **a** but for the summer scPDSI index. The hatching highlights significant correlation coefficients at a confidence level of 95%. Analyzed period: 1901–2014

δ^{18}O ratios by modulating the prevailing large-scale circulation and the occurrence of droughts and heatwaves. Thus, the local tree ring δ^{18}O variability can be explained, at least partially, via the ocean–atmosphere interaction.

4 Conclusions

The calibration and verification results demonstrate that δ^{18}O values of the latewood cellulose of oak trees from Romania are a very good proxy indicator for local summer relative humidity and could be used to provide a long record of summer droughts. Spatial correlation analysis reveals that the δ^{18}O values also contain information on atmospheric circulation at a European scale, characterized by a dipole structure: negative correlations with drought conditions over the central and the eastern part of Europe and positive correlations with wet conditions over Fennoscandia. The internal variability of δ^{18}O values relates to large-scale summer atmospheric circulation, with high δ^{18}O values associated with anticyclonic circulation, drought and heat waves over the central and eastern part of Europe. There is considerable potential to produce long and well-replicated oak tree ring stable isotope chronologies in Romania which would allow reconstructions of both regional drought and large-scale circulation variability over southern and central Europe.

Acknowledgements The research leading to these results has received funding from EEA Financial Mechanism 2009–2014 under the project contract no CLIMFOR18SEE. M. Ionita was funded by the Helmholtz Climate Initiative REKLIM. NJL and DMcC acknowledge support from the UK NERC NE/P011527/1.

References

Árvai M, Morgós A, Kern Z (2018) Growth-climate relations and the enhancement of drought signals in pedunculate oak (*Quercus robur* L.) tree-ring chronology in Eastern Hungary. iForest Biogeosci For 11:267–274. https://doi.org/10.3832/ifor2348-011

Boettger T, Haupt M, Knöller K et al (2007) Wood cellulose preparation methods and mass spectrometric analyses of δ^{13}C, δ^{18}O, and nonexchangeable δ^{2}H values in cellulose, sugar, and starch: an interlaboratory comparison. Anal Chem 79:4603–4612. https://doi.org/10.1021/ac0700023

Compo GP, Whitaker JS, Sardeshmukh PD (2006) Feasibility of a 100-year reanalysis using only surface pressure data. Bull Am Meteorol Soc 87:175–190. https://doi.org/10.1175/BAMS-87-2-175

Compo GP, Whitaker JS, Sardeshmukh PD et al (2011) The twentieth century reanalysis project. Q J R Meteorol Soc 137:1–28. https://doi.org/10.1002/qj.776

Coplen TB (1994) Reporting of stable hydrogen, carbon, and oxygen isotopic abundances. Pure Appl Chem 66:273–276. https://doi.org/10.1351/pac199466020273

Dansgaard W (1964) Stable isotopes in precipitation. Tellus. https://doi.org/10.3402/tellusa.v16i4.8993

Feudale L, Shukla J (2011) Influence of sea surface temperature on the European heat wave of 2003 summer. Part II: a modeling study. Clim Dyn 36:1705–1715. https://doi.org/10.1007/s00382-010-0789-z

Gagen MH, Mccarroll D, Loader N, Robertson I (2011) Stable isotopes in dendroclimatology: moving beyond "Potential", 11th edn. Springer, Dordrecht

Gat JR (1996) Oxygen and hydrogen isotopes in the hydrologic cycle. Annu Rev Earth Planet Sci 24:225–262. https://doi.org/10.1146/annurev.earth.24.1.225

Gessler A, Brandes E, Keitel C et al (2013) The oxygen isotope enrichment of leaf-exported assimilates—does it always reflect lamina leaf water enrichment? New Phytol 200:144–157. https://doi.org/10.1111/nph.12359

Grudd H (2008) Torneträsk tree-ring width and density AD 500–2004: a test of climatic sensitivity and a new 1500-year reconstruction of north Fennoscandian summers. Clim Dyn 31:843–857. https://doi.org/10.1007/s00382-007-0358-2

Harris I, Jones PD, Osborn TJ, Lister DH (2013) Updated high-resolution grids of monthly climatic observations—the CRU TS3. 10 Dataset. Int J Climatol. https://doi.org/10.1002/joc.3711

Haupt M, Weigl M, Grabner M, Boettger T (2011) A 400-year reconstruction of July relative air humidity for the Vienna region (eastern Austria) based on carbon and oxygen stable isotope ratios in tree-ring latewood cellulose of oaks (*Quercus petraea* Matt. Liebl.). Clim Change 105:243–262. https://doi.org/10.1007/s10584-010-9862-1

Holmes RL (1983) Computer-assisted quality control in tree-ring dating and measurement. Tree Ring Bull 43:69–75

Huber DG, Gulledge J (2011) Extreme weather and climate change understanding the link, managing the risk. Sci Impacts Progr Center Clim Energy Solut. https://doi.org/10.1002/hyp.7574

Ionita M (2015) Interannual summer streamflow variability over Romania and its connection to large-scale atmospheric circulation. Int J Climatol 35:4186–4196. https://doi.org/10.1002/joc.4278

Ionita M, Lohmann G, Rimbu N et al (2012) Interannual to decadal summer drought variability over Europe and its relationship to global sea surface temperature. Clim Dyn 38:363–377. https://doi.org/10.1007/s00382-011-1028-y

Ionita M, Tallaksen LM, Kingston D et al (2017) The European 2015 drought from a hydrological perspective. Hydrol Earth Syst Sci 21:1397–1419. https://doi.org/10.5194/hess-21-3001-2017

Jones PD, Mann ME (2004) Climate over past millenia. Rev Geophys 42:1–42. https://doi.org/10.1029/2003RG000143.CONTENTS

Kalnay E, Kanamitsu M, Kistler R et al (1996) NCAR 40-year reanalysis project. Bull Am Meteorol Soc 77:437–470

Kern Z, Popa I (2016) Dendrochronological and radiocarbon analyses of subfossil oaks from the foothills. Geochronometria 43:113–120. https://doi.org/10.1515/geochr-2015-0038

Kern Z, Patkó M, Kázmér M et al (2012) Multiple tree-ring proxies (earlywood width, latewood width and delta 13 C) from pedunculate oak (*Quercus robur* L.), Hungary. Quart Int. https://doi.org/10.1016/j.quaint.2012.05.037

Kingston DG, Fleig AK, Tallaksen LM, Hannah DM (2013) Ocean–atmosphere forcing of summer streamflow drought in Great Britain. J Hydrometeorol 14:331–344. https://doi.org/10.1175/JHM-D-11-0100.1

Kingston DG, Stagge JH, Tallaksen LM, Hannah DM (2015) European-scale drought: understanding connections between atmospheric circulation and meteorological drought indices. J Clim 28:505–516. https://doi.org/10.1175/JCLI-D-14-00001.1

Kłusek M, Melvin TM, Grabner M (2015) Multi-century long density chronology of living and sub-fossil trees from Lake Schwarzensee, Austria. Dendrochronologia 33:42–53. https://doi.org/10.1016/j.dendro.2014.11.004

Labuhn I, Daux V, Pierre M et al (2014) Tree age, site and climate controls on tree ring cellulose $\delta^{18}O$: a case study on oak trees from south-western France. Dendrochronologia 32:78–89. https://doi.org/10.1016/j.dendro.2013.11.001 doi

Labuhn I, Daux V, Girardclos O et al (2016) French summer droughts since 1326 CE: a reconstruction based on tree ring cellulose $\delta^{18}O$. Clim Past 12:1101–1117. https://doi.org/10.5194/cp-12-1101-2016 doi

Laumer W, Andreu L, Helle G et al (2009) A novel approach for the homogenization of cellulose to use micro-amounts for stable isotope analyses. Rapid Commun Mass Spectrom 23:1934–1940

Leavitt SW (2010) Tree-ring C–H–O isotope variability and sampling. Sci Total Environ 408:5244–5253. https://doi.org/10.1016/j.scitotenv.2010.07.057

Levanič T, Popa I, Poljanšek S, Nechita C (2013) A 323-year long reconstruction of drought for SW Romania based on black pine (*Pinus nigra*) tree-ring widths. Int J Biometeorol 57:703–714. https://doi.org/10.1007/s00484-012-0596-9

Loader NJ, Robertson I, Barker AC et al (1997) An improved technique for the batch processing of small wholewood samples to α-cellulose. Chem Geol 136:313–317. https://doi.org/10.1016/S0009-2541(96)00133-7

Luterbacher J, Werner JP, Smerdon JE et al (2016) European summer temperatures since Roman times. Environ Res Lett 11:024001. https://doi.org/10.1088/1748-9326/11/2/024001 doi

McCarroll D (2015) "Study the past, if you would divine the future": a retrospective on measuring and understanding quaternary climate change. J Quart Sci 30:154–187. https://doi.org/10.1002/jqs.2775

McCarroll D, Loader NJ (2004) Stable isotopes in tree rings. Quart Sci Rev 23:771–801. https://doi.org/10.1016/j.quascirev.2003.06.017

McCarroll D, Pettigrew E, Luckman A et al (2002) Blue reflectance provides a surrogate for latewood density of high-latitude pine tree rings. Arct Antarct Alpine Res 4:450–453

NCR (2006) Surface temperature reconstructions for the last 2000 years. National Academies Press, Washington, DC

Nechita C (2014) The dendroclimatic signal in *Quercus robur*. Analele Univeristății din Oradea. Facultatea Protecția Mediului 23:509–516

Nechita C, Popa I (2012) The relationship between climate and radial growth for the oak (*Quercus robur* L.) in the western plain of Romania. Carpathian J Earth Environ Sci 7:137–144

Nechita C, Popa I, Eggertsson Ó (2017) Climate response of oak (Quercus spp.), an evidence of a bioclimatic boundary induced by the Carpathians. Sci Total Environ 599–600:1598–1607. https://doi.org/10.1016/j.scitotenv.2017.05.118

Peixoto JP, Oort AH (1992) Physics of climate. Springer, New York

Popa I, Bouriaud O (2013) Reconstruction of summer temperatures in Eastern Carpathian Mountains (Rodna Mts, Romania) back to AD 1460 from tree-rings. Int J Climatol. https://doi.org/10.1002/joc.3730

Popa I, Kern Z (2009) Long-term summer temperature reconstruction inferred from tree ring records from the Eastern Carpathians. Clim Dyn 32:1107–1117

Popa I, Sidor C (2010) Rețeua romaneasca de dendrocronologie RODENDRONET 1. Conifere. Editura Silvica

Puchałka R, Koprowski M, Gričar J, Przybylak R (2017) Does tree-ring formation follow leaf phenology in Pedunculate oak (*Quercus robur* L.)? Eur J For Res 136:259–268. https://doi.org/10.1007/s10342-017-1026-7

Dalgaard P, R Development Core Team (2010) R: a language and environment for statistical computing. Computer programme, Retrieved from http://www.R-project.org/

Rădoane M, Nechita C, Chiriloaei F et al (2015) Late Holocene fluvial activity and correlations with dendrochronology of subfossil trunks: Case studies of northeastern Romania. Geomorphology 239:142–159. https://doi.org/10.1016/j.geomorph.2015.02.036

Rayner NA (2003) Global analyses of sea surface temperature, sea ice, and night marine air temperature since the late nineteenth century. J Geophys Res 108:4407. https://doi.org/10.1029/2002JD002670

Roden J, Lin G, Ehleringer JR (2000) A mechanistic model for interpretation of hydrogen and oxygen isotope ratios in tree-ring cellulose. Geochim Cosmochim Acta 64:21–35

Schubert SD, Wang H, Koster RD et al (2014) Northern Eurasian heat waves and droughts. J Clim 27:3169–3207. https://doi.org/10.1175/JCLI-D-13-00360.1

Schweingruber FH (1988) Tree rings: basics and applications of dendrochronology. Springer, Netherlands

Schweingruber FH (1996) Tree rings and environment: dendroecology. Swiss Federal Institute for Forest, Snow and Landscape Research, Birmensdorf

Smerdon JE, Pollack HN (2016) Reconstructing Earth's surface temperature over the past 2000 years: the science behind the headlines. Wiley Interdiscip Rev Clim Change 7:746–771. https://doi.org/10.1002/wcc.418

Spinoni J, Lakatos M, Szentimrey T et al (2015) Heat and cold waves trends in the Carpathian Region from 1961 to 2010. Int J Climatol 35:4197–4209. https://doi.org/10.1002/joc.4279

Treydte K, Boda S, Graf Pannatier E et al (2014) Seasonal transfer of oxygen isotopes from precipitation and soil to the tree ring: source water versus needle water enrichment. New Phytol 202:772–783. https://doi.org/10.1111/nph.12741

Van Lanen HAJ, Laaha G, Kingston DG et al (2016) Hydrology needed to manage droughts: the 2015 European case. Hydrol Process 30:3097–3104. https://doi.org/10.1002/hyp.10838

van Lanen RJ, Groenewoudt BJ, Spek T, Jansma E (2016) Route persistence. Modelling and quantifying historical route-network stability

from the Roman period to early-modern times (AD 100–1600): a case study from the Netherlands. Archaeol Anthropol Sci. https://doi.org/10.1007/s12520-016-0431-z

Whitaker JS, Compo GP, Wei X, Hamill TM (2004) Reanalysis before radiosondes using ensemble data assimilation. Bull Am Meteorol Soc 132:2983–2991. https://doi.org/10.1175/1520-0493(2004)132%3C1190:RWRUED%3E2.0.CO;2

Wilson R, Rao R, Rydval M et al (2014) Blue intensity for dendroclimatology: the BC blues: a case study from British Columbia, Canada. Holocene 24:1428–1438. https://doi.org/10.1177/0955968361454405 1

Young GHF, Loader NJ, McCarroll D et al (2015) Oxygen stable isotope ratios from British oak tree-rings provide a strong and consistent record of past changes in summer rainfall. Clim Dyn 45:3609–3622. https://doi.org/10.1007/s00382-015-2559-4